Theor Chem Acc (2010) 127:327–344
DOI 10.1007/s00214-009-0720-z

REGULAR ARTICLE

Thermal unimolecular decomposition mechanism of 2,4,6-trinitrotoluene: a first-principles DFT study

Xiao-Fang Chen · Ji-Feng Liu · Zi-Hui Meng · Ke-Li Han

Received: 9 September 2009 / Accepted: 13 December 2009 / Published online: 14 January 2010

Abstract Simple C–NO_2 homolysis, 4,6-dinitroanthranil (DNAt) production by dehydration, and the nitro-nitrite rearrangement–homolysis for gas-phase TNT decomposition were recently studied by Cohen et al. (J Phys Chem A 111:11074, 2007), based on DFT calculations. Apart from those three pathways, other possible initiation processes were suggested in this study, i.e., CH_3 removal, O elimination, H escape, OH removal, HONO elimination, and nitro oxidizing adjacent backbone carbon atom. The intermediate, 3,5-dinitro-2(or 4)-methyl phenoxy, is more favor to decompose into CO and 3,5-dinitro-2(or 4)-methyl-cyclopentadienyl than to loss NO following nitro-nitrite rearrangement. Below ~1,335 K, TNT condensing to DNAt by dehydration is kinetically the most favor process, and the formations of substituted phenoxy and following cyclopentadienyl include minor contribution. Above ~1,335 K, simple C–NO_2 homolysis kinetically dominates TNT decomposition; while the secondary process changes from DNAt production to CH_3 removal above ~2,112 K; DNAt condensed from TNT by dehydration yields to that by sequential losses of OH and H above ~1,481 K and to nitro-nitrite rearrangement–fragmentation above ~1,778 K; O elimination replaces DNAt production above ~2,491 K, playing the third role in TNT decomposition; H escaping directly from TNT thrives in higher temperature (above ~2,812 K), as the fourth largest process. The kinetic analysis indicates that CH_3 removal, O elimination, and H escape paths are accessible at the suggested TNT detonation time (~100–200 fs), besides C–NO_2 homolysis. HONO elimination and nitro oxidizing adjacent backbone carbon atom paths are negligible at all temperatures. The calculations also demonstrated that some important species observed by Rogers and Dacons et al. are thermodynamically the most favor products at all temperatures, possibly stemmed from the intermediates including 4,6-dinitro-2-nitroso-benzyl alcohol, 3,5-dinitroanline, 2,6-dinitroso-4-nitro-phenylaldehyde, 3,5-dinitro-1-nitrosobenzene, 3,5-dinitroso-1-nitrobenzene, and nitrobenzene. All transition states, intermediates, and products have been indentified, the structures, vibrational frequencies, and energies of them were verified at the uB3LYP/6-311++G(d,p) level. Our calculated energies have mean unsigned errors in barrier heights of 3.4–4.2 kcal/mol (Lynch and Truhlar in J Phys Chem A 105:2936, 2001), and frequencies have the recommended scaling factors for the B3-LYP/6-311+G(d,p) method (Andersson and Uvdal in J Phys Chem A 109:2937, 2005; Merrick et al. in J Phys Chem A 111:11683, 2007). All calculations corroborate highly with the previous experimental and theoretical results, clarifying some pertinent questions.

Keywords Nitroaromatics · 2,4,6-Trinitrotoluene (TNT) · Energetic materials · Density function theory · Thermal decomposition

Electronic supplementary material The online version of this article (doi:10.1007/s00214-009-0720-z) contains supplementary material, which is available to authorized users.

X.-F. Chen · J.-F. Liu · K.-L. Han (✉)
State Key Laboratory of Molecular Reaction Dynamics,
Dalian Institute of Chemical Physics,
Chinese Academy of Sciences,
116023 Dalian, People's Republic of China
e-mail: klhan@dicp.ac.cn
URL: http://www.beam.dicp.ac.cn

Z.-H. Meng
Department of Chemical and Environmental Engineering,
Beijing Institute of Technology, 100081 Beijing,
People's Republic of China

1 Introduction

2,4,6-Trinitrotoluene (TNT) is one of the essential energetic poly nitroarenes as an explosive and propellant, renowned for its compatibility with other materials, low hygroscopicity, low melting point, low cost, relatively low sensitivity to impact and friction, good thermal stability, and powerful explosive force [1, 2]. In recent decades, much progress has been made in understanding the chemical and physical properties of TNT and other nitroaromatic compounds, especially in thermal decomposition products. Most experiments agree on the final products, including anthranil, alcohol, aldehyde, aniline, carboxylic acid, nitroso, oxime, nitrile, nitrone, nitroxide, azo, and azoxy groups in the condensed-phase residue [2–11].

Rogers [4] found that the TNT and volatile impurities begin to vaporize and appear on the thin-layer chromatography plate between 125 and 135 °C, when a TNT sample was exposed to programming heat (100–370 °C) under air. He also observed that the principal partial decomposition products include 2,4,6-trinitrobenzyl alcohol, 4,6-dinitroanthranil, 2,4,6-trinitrobenzoic acid, 1,3,5-trinitrobenzene, and 2,4,6-trinitrobenzaldehyde (trace). Of them, 2,4,6-trinitrobenzoic acid and 1,3,5-trinitrobenzene are the first and the last products to disappear from the record, respectively. However, Dacons et al. [11] did not detect 1,3,5-trinitrobenzene from the isothermal decomposition of TNT at 200 °C. The complex products observed by Rogers necessitate the rupture of the methyl C–H bond in the initial stages of decomposition of TNT. A primary deuterium isotope effect (KIE) (~1.66) was provided for supporting the critical C–H bond rupture by Shackelford et al. [12] from the isothermal differential scanning calorimetric (DSC) experiments on the thermal decomposition of liquid TNT. Besides, the dimeric reduction product of TNT containing azo or azoxy linkage with undisturbed methyl groups (Fig. 1a) were isolated and identified in the early radical-producing step in TNT decomposition [4, 11].

Many researchers have reported the formation of electron paramagnetic resonance (EPR) spectra of free radicals during photolysis and thermolysis of TNT [13–16]. It was concluded that radicals are present in the initial and later stages of the thermochemical decomposition of TNT. The earliest observed radical produced in photochemical decompositions of TNT can be attributed to an aryl benzyl

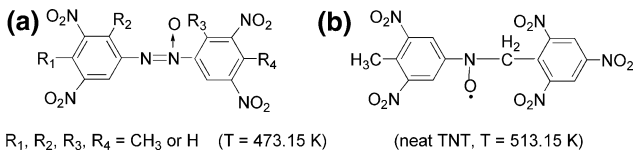

Fig. 1 Dimeric reduction products of TNT decomposition reported in experiments

nitroxide moiety (Fig. 1b). The evidence of the initial formation of 2,4,6-trinitrobenzyl anion also appears in the photolysis of aqueous solutions of TNT [17].

Mass spectral fragmentation schemes were reported for TNT in numerous experiments [3, 18–23]. Carper et al. [19] and Yinon [20] observed that the major pathways of TNT include the loss of OH or H_2O, followed by the subsequent loss of NO or NO_2 in collision-induced dissociation (CID) tandem mass spectrometry (MS/MS). Later, Yinon et al. [21] examined that TNT was characterized by loss of OH, NO, and NO_2 in electron spray ionization tandem mass spectrometry (ESI/MS). Loss of OH was presumably due to the *ortho* effect. Loss of HNO_2 from TNT was also found by Yinon et al. [21] and Hankin et al. [22] in the CID and EI spectrometry. Recently, Martin et al. [23] reported that a peak at m/z −226 attributed to $[TNT–H]^-$ is most prevalent in the low-energy (e.g., 0.7 nJ/μm^2) single-particle mass spectra of aerosolized TNT, but is still visible even at the high-energy fluency of 2.66 nJ/μm^2 although its intensity decreasing, due to the loss of the nitrate groups and the breaking of the aromatic ring; several other high mass peaks assigned to $[TNT–CH_3]^-$, $[TNT–OH]^-$ $[TNT–NO]^-$ which are distinct in the low energy become weaker with the enhancement of the laser energy, possibly owe to the extensive fragmentation.

The structural properties of TNT had been investigated extensively in the previous studies based on the semi-empirical (MINDO/3 and MNDO) approximations and density function theory (DFT), in combination with X-ray studies [24, 25]. Crystals of TNT are orthorhombic, and two unique molecules exist within the unit cell. The discrepancies in the two molecules lie only in orientations of the 2 and 6 nitro groups, and the methyl group [25]. Using 1-nitropropene as a model, Turner et al. [26, 27] and Cox et al. [28] proposed several thermal unimolecular decomposition reaction channels of TNT, such as hydrogen atom transfer, nitro group removal, nitro-nitrite rearrangement, and HONO elimination. Recently, Cohen et al. [29] reported a direct investigation of TNT decomposition. They predicted that at relatively low temperatures, 2,4-dinitroanthranil production initial from intra-H transfer is both kinetically and thermodynamically the most favorable pathway, while the C–NO_2 homolysis becomes dominates TNT decomposition at ~1,250–1,500 K; nitro-nitrite rearrangement–homolysis is kinetically unfavorable when compared with the other two pathways at all temperatures, although it thermodynamically favors over the C–NO_2 homolysis at room temperature and is the most exergonic pathway at high temperatures; only the NO_2 homolysis pathway is kinetically accessible at the estimated detonation time scale (100–200 fs) [24, 29–31].

The activation energies from several experimental studies are 39–53 and 30–35 kcal/mol for the induction

phase (–CH_3 oxidation) and acceleratory phase (catalyst dominated) during TNT decomposition, respectively [2, 10, 12, 14] and their remarkable discrepancy is clearly altered by the experimental conditions, and they do not reflect the true kinetics of TNT. In addition, the observed decomposition products vary greatly according to diverse experimental conditions, such as heating rate, sample dimensions, experimental instruments, and composition of the surrounding matrix. It must be indicated that TNT fragmentation patterns and its mass spectrometry may possibly be related, but not equivalent, after all the former associates with the neutral molecule while the latter with the cation or anion. Moreover, it is difficult to detect the more reactive intermediates that are central to the decomposition mechanism at elevated temperatures and would rearrange and react further. Although the large volume of data that have been accumulated is fundamental for exploring the mechanisms of TNT, adequate, and theoretically direct data are still needed. In this paper, numerous alterative sources of some experimentally observed species are considered, most of which have not been mentioned in previous theoretical studies [24–29]. The study of the thermal decomposition of TNT can be useful in understanding the behavior of explosives in the initial stages of decomposition and in the propagation steps for detonation, and for analysis of environmental sample to govern explosives-contaminated sites.

2 Computational methods

For insight into the decomposition mechanism of TNT, electronic structure calculations were performed with the Gaussian 03 suite of programs [32]. The geometries of the reactants, products, intermediates, and transition states (TS) were calculated at the level of uB3LYP hybrid Hartree–Fock nonlocal approach of Becke in conjugation with 6-311++G(d,p) basis set [33–39]. The density function theory (DFT) has been universally applied to study some well-known energetic materials, e.g., TNT [29], hexahydro-1,3,5-trinitro-*s*-triazine (RDX) [40, 41], 1,3,5,7-tetranitro-1,3,5,7-tetraazacycloocatne (HMX) [42], and 1,3,3-trinitroazetidine (TNAZ) [43], because of their large molecular weights. Some reports indicated that this theory method has means unsigned errors in barrier heights of 3.4–4.2 kcal/mol [44], and its new scale factors can be chosen as 0.9688 (or 0.9679) for vibrational frequencies, 1.0189 (or 1.0100) for low-frequency vibrations, and 0.9877 (or 0.9887) for zero-point vibrational energies (ZPVE) [45, 46]. Therefore, this calculation level containing diffuse function [39] and polarization function [47] in this paper was chosen to be consistent with practical extension and proper accuracy. In addition, all transition states reported here have only one imaginary frequency, and are located without imposing any symmetry constraints during the geometry optimization process. In all cases, all transition states have been positively verified to connect a specific pair of stationary points (reactants, products, or minima associated with intermediate species) by performing the necessary intrinsic reaction coordinates (IRC) calculations [48, 49]. Harmonic frequencies and zero-point energies (ZPEs) were calculated with analytical force constants at all the optimized geometries. TNT has two structures [25], but structure A was chosen as the reference for the energies of other species in the unimolecular decomposition. All energies in this study have been with ZPE or thermal correlations.

3 Results and discussion

Schemes 1, 2, and 3 illustrate the formation of 4,6-dinitroanthranil, the degradation of 4,6-dinitro-2-nitrosobenzyl alcohol (*17*), and the reaction routes for TNT decomposition, respectively. Figure 2 shows a generalized scheme of Boulton–Ktritzky rearrangement (BKR) [50]. Figure 3 provides simple structures of species *1–117* for transition states, intermediates and some important products in the unimolecular decomposition and dissociation of TNT. Figures 4, 6, and 8 are the relative enthalpy (ΔH) and Gibbs free energy (ΔG) diagram for the decomposition and dissociation reactions of TNT at uB3LYP/6-311++G(d,p), respectively, in comparison with the results reported by Cohen et al. [29]. Figures 5, 7, and 9 are the relative enthalpy (ΔH) and Gibbs free energy (ΔG) diagram for the degradation of the important intermediate *17* during TNT decomposition, respectively, as calculated at uB3LYP/6-311++G(d,p). Figures 10 and 11 show the enthalpy/Gibbs free energy differences ($\Delta\Delta H(T)/\Delta\Delta G(T)$) at the specified temperature (T). Figure 12 represents the dependence between relative Gibbs free energy (ΔG) and temperature (T). Figure 13 shows Arrhenius plot ($\ln k$ vs. $1/T$) for TNT decomposition pathways. Table 1 gives the relative entropies (ΔS) at 298 K for some important species. Tables 2 and 3 contain 20 main reactions of TNT decomposition and their relative importance, respectively. The optimized geometries (*XYZ* coordinates) and harmonic

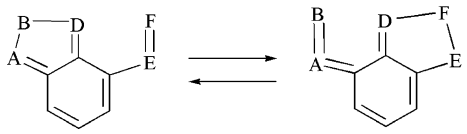

Fig. 2 A generalized scheme of the Boulton–Katritzky rearrangement: A, E = N, N^+–O^-, N^+–N^-R, CR; B, F = O, NR, S; D = N, CR

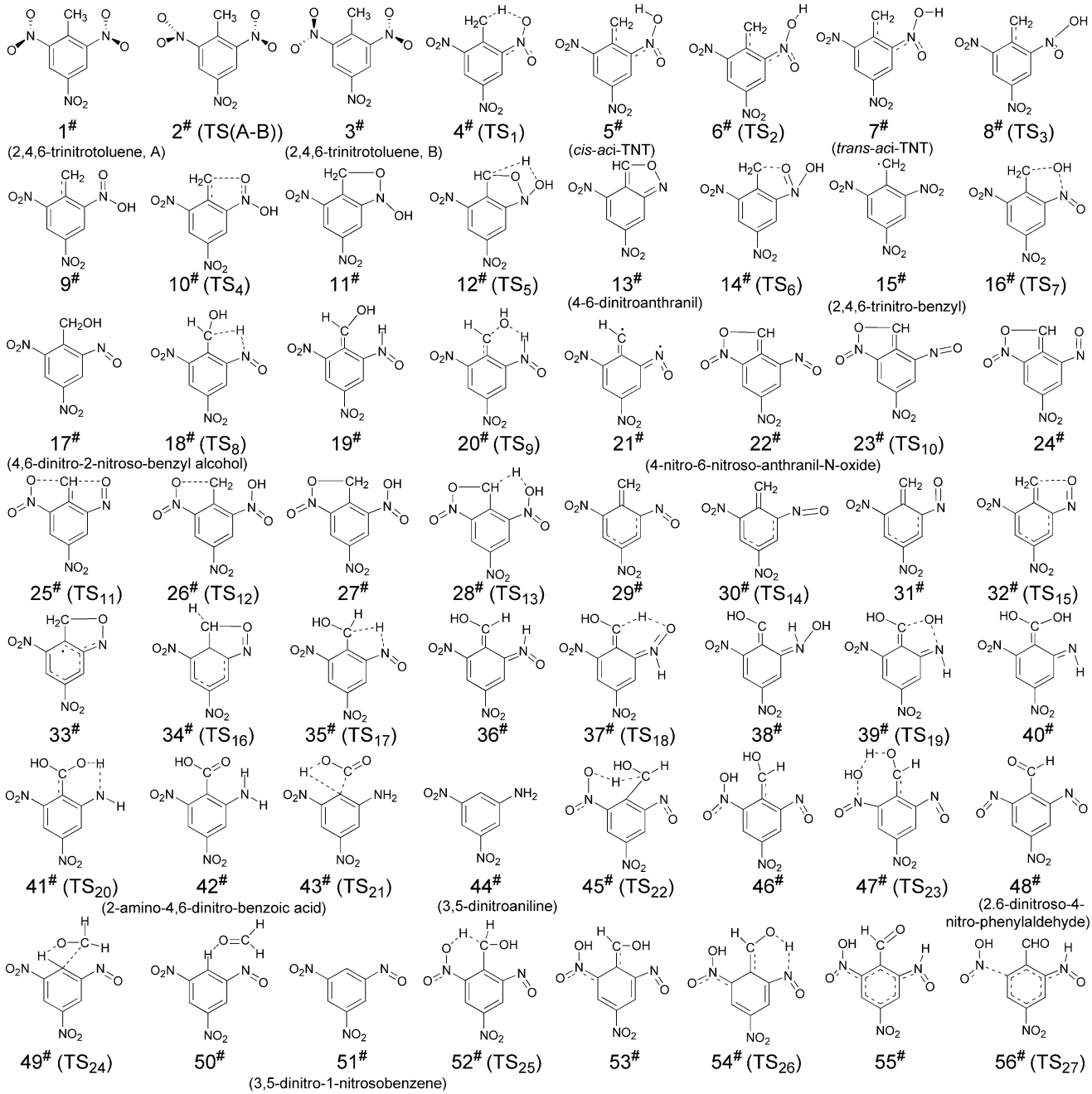

Fig. 3 Species *1–117* related to the unimolecular decomposition and dissociation reactions of TNT

frequencies for all stationary points are included as supplementary material.

3.1 Equilibrium structure of TNT

As shown in Fig. 3, TNT exhibits two genuine energy minimum structures. In structure A (*1*), the 2 and 6 nitro groups are almost in the same cross section, both twisted slightly out of the phenyl ring plane by 40.9°, whereas they are in a scissor configuration in the phenyl ring plane's view in structure B (*3*), diverged from the phenyl ring plane by 41.3° and 52.1°, respectively. Attentively, the 4-position nitro group in A or B is nearly planar to the benzene ring. The twisted phenomena of the 2 and 6 nitro groups contribute to steric interaction with the methyl group. The conformer A of TNT is preferential to the conformer B by the internal energy of 0.518 kcal/mol, and A is closest to that observed in the crystal structures of

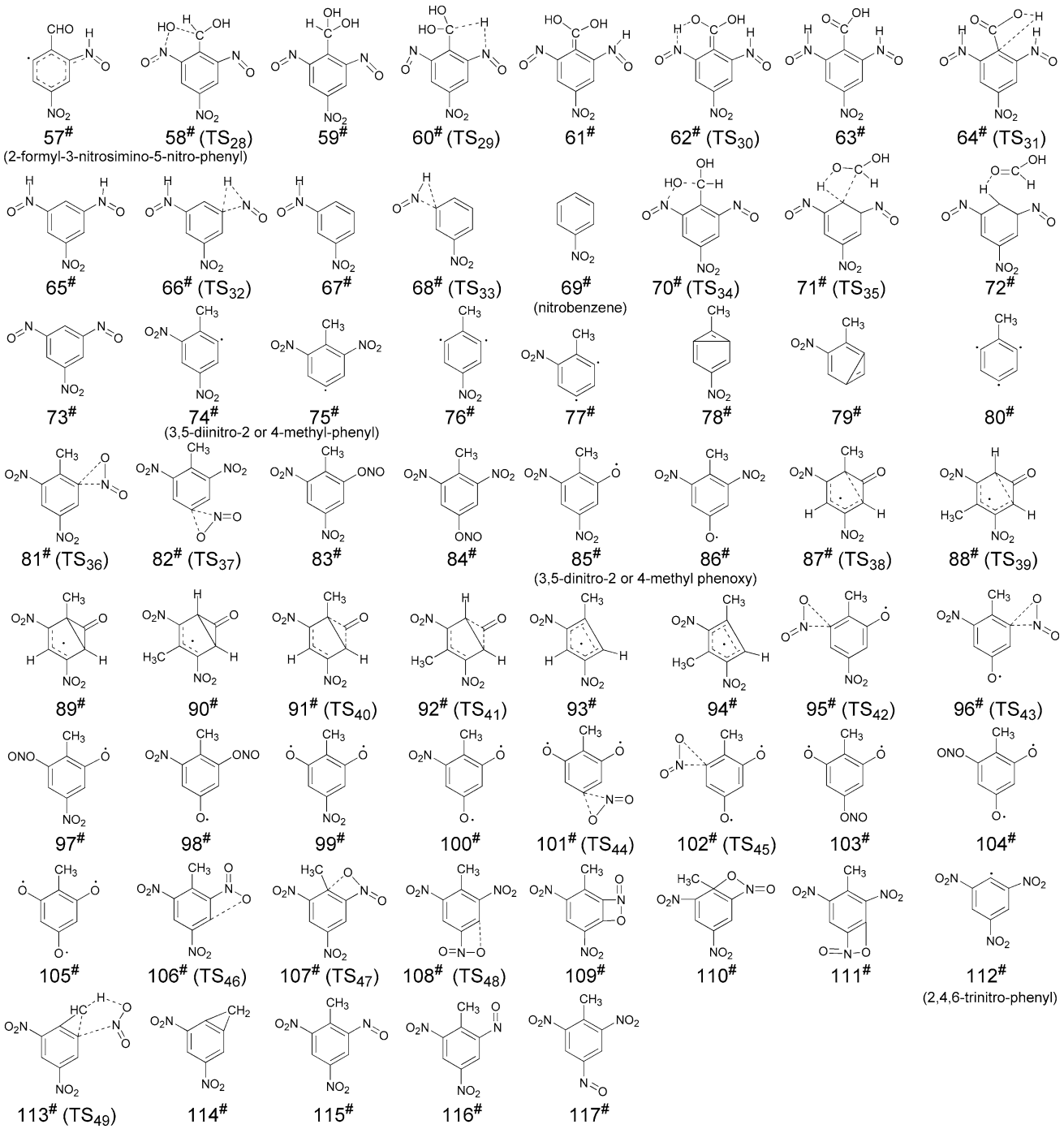

Fig. 3 continued

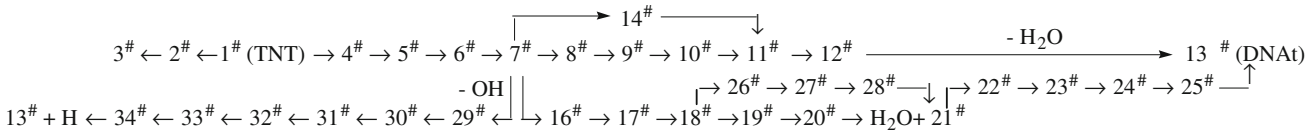

Scheme 1 2,4,6-trinitrotoluene (TNT) condensing to 4,6-dinitroanthranil (DNAt). The species are shown in Fig. 3

TNT [24]. The transition state, TS(A–B) (*2*), corresponds to interconversion between them, with the internal energy of 1.106 kcal/mol over the conformer A. Analytically, the vibrational model with imaginary frequency (57i cm^{-1}) of TS(A–B) is mainly internal rotation of 6-position nitro, involving slightly concerted motion of internal rotations 2-position nitro and methyl. Thus, this interconversion is also a "cog wheel" type of mechanism.

3.2 Isomerization and dissociation of TNT

3.2.1 The intramolecular hydrogen (intra-H) transfer path

The hydrogen atom of methyl in TNT is activated by the *ortho* nitro group, and then transfers to the N atom in *ortho*-NO_2 via a cyclic activated complex TS_1 (*4*), leading to a short-lived *cis* of *aci*-tautomer of TNT (*cis-aci*-TNT)

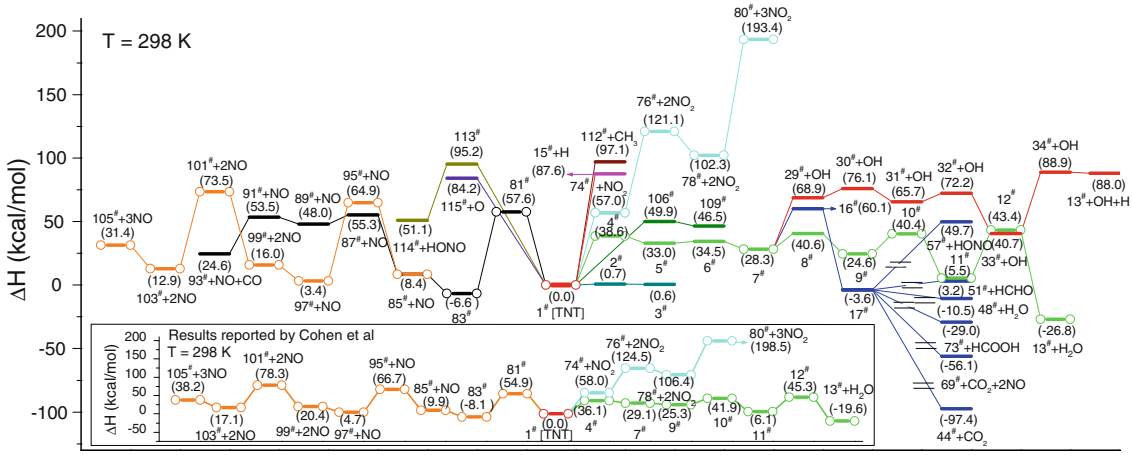

Fig. 4 Relative enthalpy (ΔH) diagram at room temperature for the decomposition and dissociation reactions of TNT, as calculated at the uB3LYP/6-311++G(d,p) level. *Inset* illustrates the results reported by Cohen et al. at the uB3LYP/cc-PVDZ level. The *values in parenthesis* are the sum of electronic and thermal enthalpies (ΔH) at 298 K relative to TNT. *Each color line* represents one type of reaction route. The reaction routes are referred to Schemes 1, 2, and 3, but transition states and intermediates in the reactions of $17^{\#} \rightarrow 44^{\#} + CO_2$, $17^{\#} \rightarrow 48^{\#} + H_2O$, $17^{\#} \rightarrow 51^{\#} + HCHO$, $17^{\#} \rightarrow 57^{\#} + HONO$, $17^{\#} \rightarrow 69^{\#} + CO_2 + 2NO$, and $17^{\#} \rightarrow 73^{\#} + HCOOH$ are omitted for the sake of clarity, while their detailed information is provided in Fig. 5. The C–NO_2 homolysis and nitro-nitrite rearrangement of TNT in the *para* position, and two optional processes in the O elimination and nitro oxidizing adjacent backbone carbon atom pathways are omitted for the sake of clarity, and their detailed information are provided in supplementary material. *The lines with cycles* mean that the corresponding species were mentioned by Cohen et al.

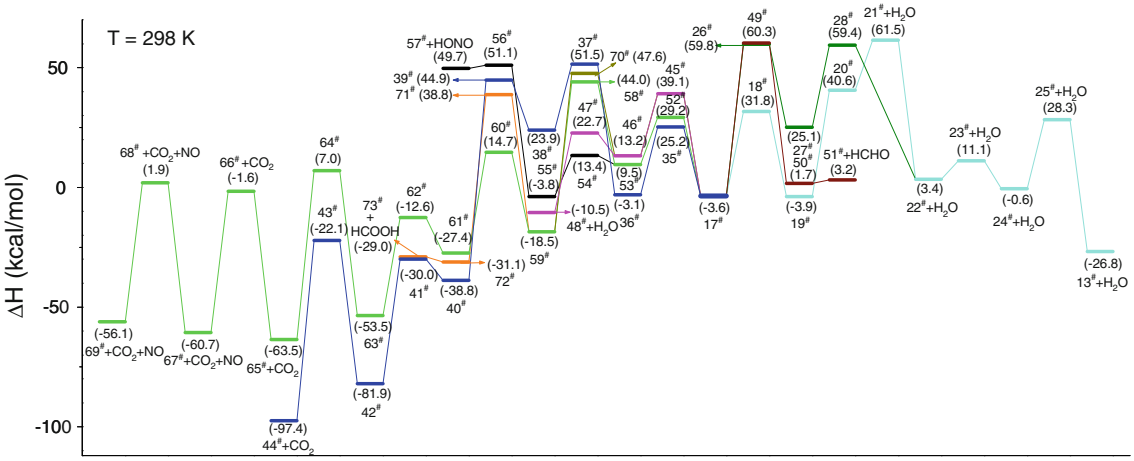

Fig. 5 Relative enthalpy (ΔH) diagram at room temperature for the degradation of the important intermediate 4,6-dinitro-2-nitroso-benzyl alcohol (*17*) during TNT decomposition, as calculated at uB3LYP/6-311++G(d,p). The *values in parenthesis* are the sum of electronic and thermal enthalpies (ΔH) at 298 K relative to TNT. The reaction routes are referred to Schemes 1 and 2

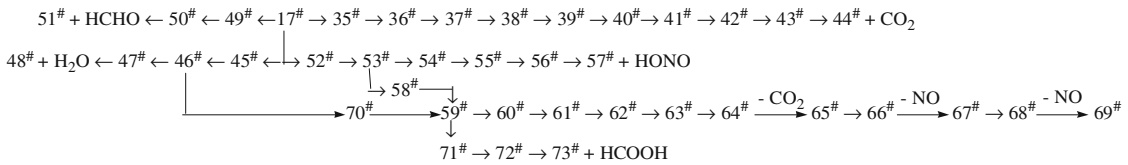

Scheme 2 The important intermediate 4,6-dinitro-2-nitroso-benzyl alcohol (*17*) facilitating the conversion into a radical (*57*) and other low-energy species, including 3,5-dinitroanline (*44*), 2,6-dinitroso-4-nitro-phenylaldehyde (*48*), 3,5-dinitro-1-nitrosobenzene (*51*), nitrobenzene (*69*), and 3,5-dinitroso-1-nitrobenzene (*73*). The species are shown in Fig. 3

(5). The *cis–trans* conversion in *aci*-TNT occurs by the internal torsion of hydroxyl group. The *trans-aci*-TNT (*7*) is likely to condense to 4,6-dinitroanthranil (DNAt) (*13*) by dehydration or by sequential losses of OH and H. Before dehydration, a benzisoxazole derivative (*11*) is formed directly via TS_6 (*14*) or after the torsion of the nitronate group (–NOOH) via TS_3 (*8*) and following ring-closing reaction (*10*), whereas the latter is the most favorable by 6.6 kcal/mol enthalpy barrier (ΔH) at 298 K; likewise, 4-nitro-6-nitroso-anthranil *N*-oxide (*22*)—or the unstable triplet diradical (*21*) is generated via TS_9 (*20*) or TS_{13} (*28*), which is followed by the internal rotation of the nitroso group (*23*) and the Boulton–Katritzky rearrangement [50] (*24* → *25* → *13*). During *trans-aci*-TNT indirectly condensing to *22* or *21*, 4,6-dinitro-2-nitroso-benzyl alcohol (*17*) is formed by the hydroxyl migration to benzyl in *trans-aci*-TNT. *Aci*-TNT also dissociates into *29* + OH by the rupture of weak N–OH bond, and then the essential conversion of *29* into *13* + H occurs, after the internal rotation of the nitroso group via TS_{14} (*30*), sequential ring-closing reaction via TS_{15} (*32*), and H escape via TS_{16} (*34*). Alternatively, the NO–H bond in *aci*-TNT or *9* breaks down, leading to 2,4,6-trinitrobenzyl radical (*15*) + H. Scheme 1 depicts the reaction routes for the formation DNAt.

When TS_6 is ruled out as considered above, TS_5 (*12*) and TS_7 (*16*) are the rate-determining steps (RDSs) in TNT condensing to DNAt by dehydration, respectively, as shown in Figs. 4 and 5. In addition, their activation enthalpies (ΔH) are 43.4 and 60.1 kcal/mol relative to TNT at uB3LYP/6-311++G(d,p) level. Thus, the former with less steps and lower barrier dominates this multi-well decomposition process of TNT → DNAt + H_2O. Meanwhile, TS_{16} (*34*) is the RDS for DNAt condensed from TNT by sequential losses of OH and H, with an 88.9 kcal/mol activation enthalpies (ΔH) relative to TNT. This barrier is 45.5 kcal/mol above the minimum value of RDS for TNT condensing to DNAt by dehydration. Moreover, the reaction enthalpy (ΔH) of TNT → DNAt + H_2O and TNT → DNAt + H + OH pathways are −26.8 and 88.0 kcal/mol, respectively. One is exothermal, but the other is endothermal. Therefore, at room temperature (298 K), TNT condenses to DNAt both kinetically and thermodynamically by the rejection of water rather than by subsequent losses of OH and H, and the reaction route with the lowest energy barrier is *1* (TNT) → *4* → *5* → *6* → *7* → *8* → *9* → *10* → *11* → *12* → *13* (DNAt) + H_2O.

Lifshitz et al. [51] have reported that the thermal decomposition of anthranil leads to two major products (aniline and cyclopentadiene carbonitrile) and four minor products (pyridine, CH_2=CHCN, HCN and CH≡C–CN). The extensive fragmentation of DNAt is expected to show some feather in common with anthranil, its detailed information is not explored in this study.

Apart from dehydration into the important species *13*, 4,6-dinitro-2-nitroso-benzyl alcohol facilitates the conversion into a radical (*57*) and other low-energy species including 3,5-dinitroanline (*44*), 2,6-dinitroso-4-nitro-phenylaldehyde (*48*), 3,5-dinitro-1-nitrosobenzene (*51*), nitrobenzene (*69*) and 3,5-dinitroso-1-nitrobenzene (*73*) when it losing HONO, CO_2, H_2O, HCHO, CO_2 + 2NO, and HCOOH, respectively. The reaction routes are illustrated in Scheme 2. As shown in Fig. 5, the rate-determining steps for their formations from *17* are TS_{27} (*56*), TS_{18} (*37*), TS_{22} (*45*), TS_{24} (*49*), TS_{28} (*58*), and TS_{28} (*58*), with the enthalpies (ΔH) of 51.1, 51.5, 39.1, 60.3, 44.0, and 44.0 kcal/mol relative to TNT. We notice that an enthalpy barrier of 60.1 kcal/mol should be overcome when species *17* is generated form TNT, as shown in Fig. 4. Thus, species *57*, *44*, *48*, *51*, *69*, and *73*, appear much more easily, once species *17* is formed during the thermal decomposition of TNT. The products systems, *44* + CO_2, *48* + H_2O, *51* + HCHO, *69* + CO_2 + 2NO, and *73* + HCOOH, are with the enthalpies (ΔH) of −97.4, −10.5, 2.2, −56.1, and −29.0 kcal/mol relative to TNT, respectively. Especially, the release of significant net energies (ΔH) accelerates the single elementary steps of TNT condensing to *44*, *48*, *69*, and *73* in the gas phase, although involving substantial movement of many steps.

The species, *17*, *48*, and *73*, may be ones of possible intermediates in generating experimentally observed products 2,4,6-trinitrobenzalcohol, 2,4,6-trinitrobezenaldehyde (or 2,4,6-trinitro benzoic acid), and 1,3,5-trinitrobenzene [4, 11, 12], respectively, involving the uptake of

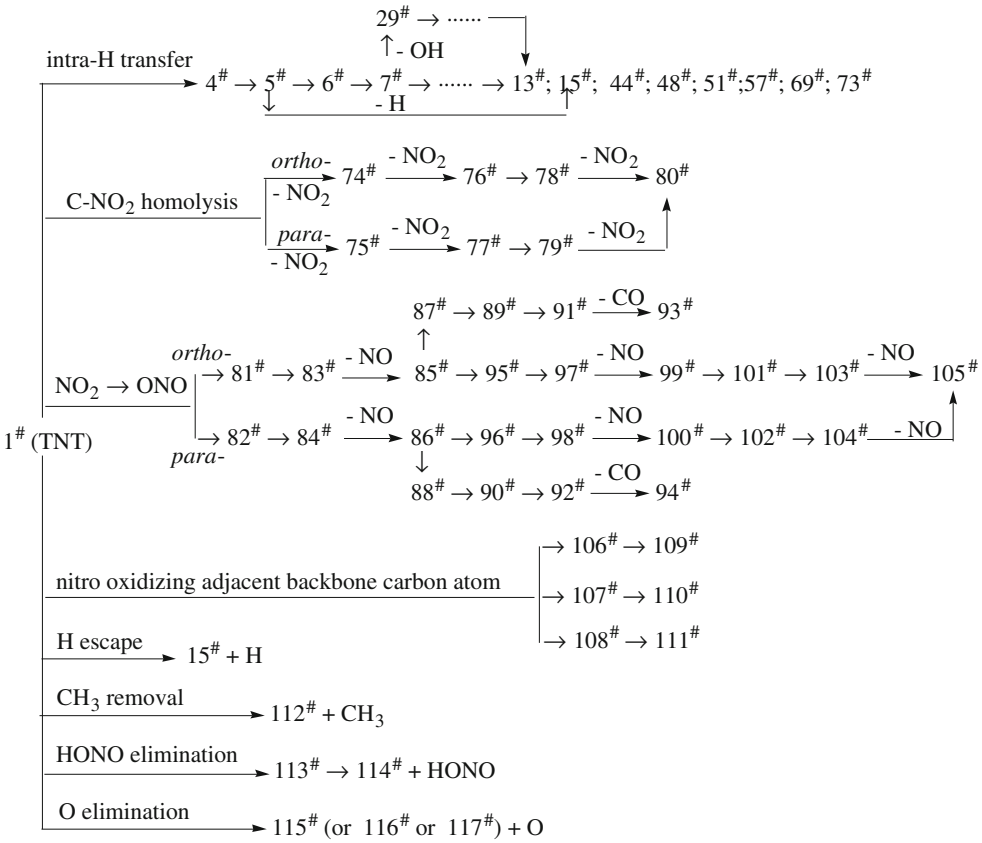

Scheme 3 Outline for the decomposition and dissociation reactions of TNT. The species are shown in Fig. 3

one or two atoms of solvent/air oxygen. The analogy with TNT condensing to *44* has been observed experimentally, for instance, the principal product for the thermal decomposition of *o*-nitrotoluene in a N_2 carrier stream or liquid benzene has been shown to be aniline, resulting from the initial formation of anthranilic acid [52–55]. Also, the previous mass spectrometry experiments indicate that decarboxylation was observed as the most frequent fragmentation reactions in 2,4-dinitrobenzoic, benzoic, and sulfonic acids [56, 57].

3.2.2 *C–NO_2 homolysis*

The C–NO_2 bond dissociation enthalpies (BDE) (ΔH) at 298 K of TNT are calculated to be 57.0 and 62.8 kcal/mol, where –NO_2 located *ortho* and *para* to –CH_3 group, respectively, as shown in Fig. 4 and supplementary material (Noting that Fig. 4 only presents the energy diagram for the dominant C–NO_2 homolysis of TNT in the *ortho* position). This is good evidence that the barrier for C–NO_2 homolysis is significantly higher than that (38.6 kcal/mol) of TNT's intra-H transfer at the first step. The similar phenomena were experimentally observed that the formation of anthranil is the dominant process in *o*-nitrotoluene (*o*-NT) decomposition, and the loss of NO_2 proceeds via loose transition states (high A factors) in single-pulse shock-tube experiments [58, 59]. In Fig. 4, inset illustrates the reported by Cohen et al. [29]. Obviously, the *ortho* C–NO_2 BDE, we calculated resembles that (58.0 kcal/mol) by Cohen et al.

In comparison, the C–NO_2 BDE of TNT is less than those (energies in kcal/mol) of other nitroarenes reported in experiments [52] [for nitrobenzene: (71.4 ± 2.0); for *o*-NT: (70.2 ± 2.5); for *p*-NT: (71.4 ± 2.3); for 2,4-DNT: (70.6 ± 2.0)], owing to one or two additional electron-withdrawing nitro group(s) in TNT reducing the electron density in aromatic ring. However, it is higher than the N–NO_2 BDE of the nitramine (e.g., RDX: 39.0 kcal/mol [41], 34.2 kcal/mol [40]; HMX: 39.8 kcal/mol [42]). For much more information about the influence of substituent nature and position on the C–NO_2 BDE in nitroarenes, refer to the recently theoretical studies [60, 61].

The experiments revealed that aromatic ring fission does not take place until most of the attached substituents are removed [2, 62]. It is likely that the subsequent C–NO_2 homolysis of the two remaining substituents will take place. As shown in Fig. 4, our calculated enthalpies (ΔH) at 298 K are 121.1 and 193.4 kcal/mol for the second and third C-NO_2 homolysis of 2-methyl-3,5-dinitrophenyl (*74*) relative to TNT, respectively.

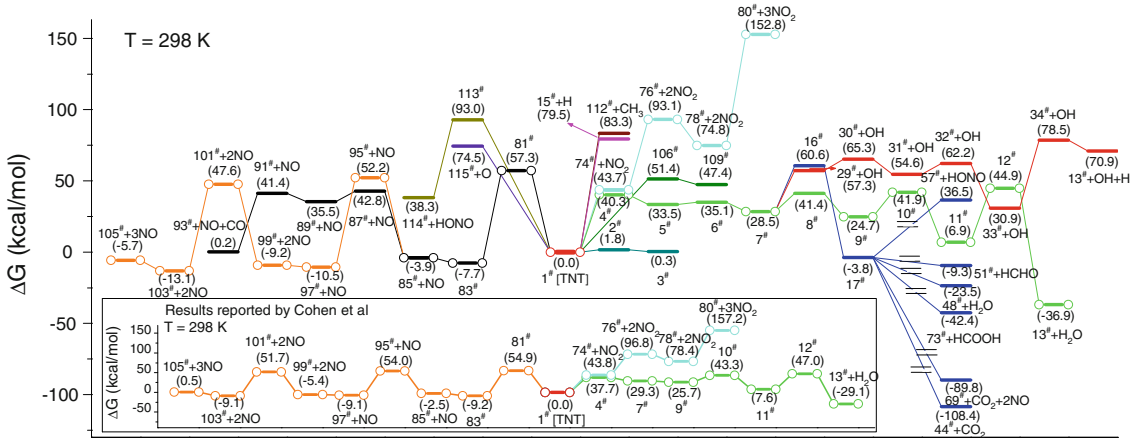

Fig. 6 Relative free energy (ΔG) diagram at room temperature for the decomposition and dissociation reactions of TNT, as calculated at uB3LYP/6-311++G(d,p). *Inset* illustrates the results reported by Cohen et al. at the uB3LYP/cc-PVDZ level. The *values in parenthesis* are the sum of electronic and thermal free energies (ΔG) relative to TNT. *Each color line* represents one type of reaction route. The reaction routes are referred to Schemes 1, 2 and 3, but transition states and intermediates in the reactions of $17^{\#} \rightarrow 44^{\#} + CO_2$, $17^{\#} \rightarrow 48^{\#} + H_2O$, $17^{\#} \rightarrow 51^{\#} + HCHO$, $17^{\#} \rightarrow 57^{\#} + HONO$, $17^{\#} \rightarrow 69^{\#} + CO_2 + 2NO$, and $17^{\#} \rightarrow 73^{\#} + HCOOH$ are omitted for the sake of clarity, while their detailed information is provided in Fig. 7. The C–NO_2 homolysis and nitro-nitroso rearrangement of TNT in the *para* position, and two optional processes in the O elimination and nitro oxidizing adjacent backbone carbon atom pathways are omitted for the sake of clarity, and their detailed information are provided in supplementary materials. *The lines with cycles* mean that the corresponding species were mentioned by Cohen et al.

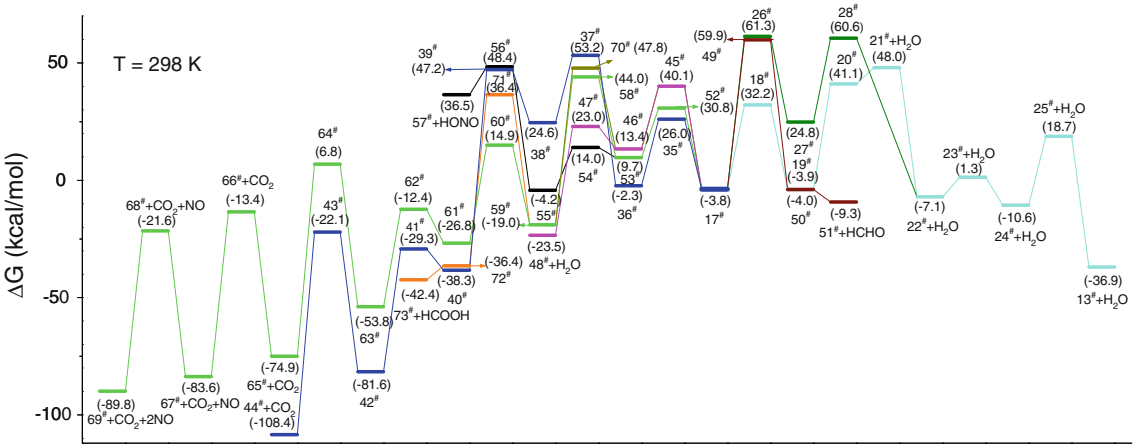

Fig. 7 Relative free energy (ΔG) diagram at room temperature for the degradation of the important intermediate 4,6-dinitro-2-nitroso-benzyl alcohol (*17*) during TNT decomposition, as calculated at uB3LYP/6-311++G(d,p). The *values in parenthesis* are the sum of electronic and thermal free energies (ΔG) at 298 K relative to TNT. The reaction routes are referred to Schemes 1 and 2

3.2.3 *Nitro-nitrite rearrangement and following fragmentation*

The nitro-nitrite isomerization on aromatic backbone will occur via a tri-centric cyclic transition states [63] (*81* and *82* in Fig. 3), overcoming 57.6 (for *ortho*) or 62.8 kcal/mol (for *para*) enthalpy barrier (ΔH) at 298 K (see Fig. 4 and supplementary material). The bond PhO–NO is weak, and nitric oxide plus 3,5-dinitro-2(or 4)-methyl phenoxy [*85* or (*86*)] will be generated by the rupture of PhO–NO in analogous aryl nitrite intermediate. This is consistent with the observation that loss of NO following nitro-nitrite rearrangement is a characteristic reaction of aromatic nitro compounds. The BDE (ΔH) of PhO–NO at 298 K is calculated to be 15.0 (or 16.2) kcal/mol for the *ortho* (or *para*) position in TNT nitrite intermediate *83* (or *84*), much less than that for nitrobenzene (22.5 kcal/mol) in previous research [64]. The 3,5-dinitro-2-methyl phenoxy (*85*) is 5.5 kcal/mol lower than 3,5-dinitro-4-methyl phenoxy (*86*) in the enthalpy at 298 K, benefited

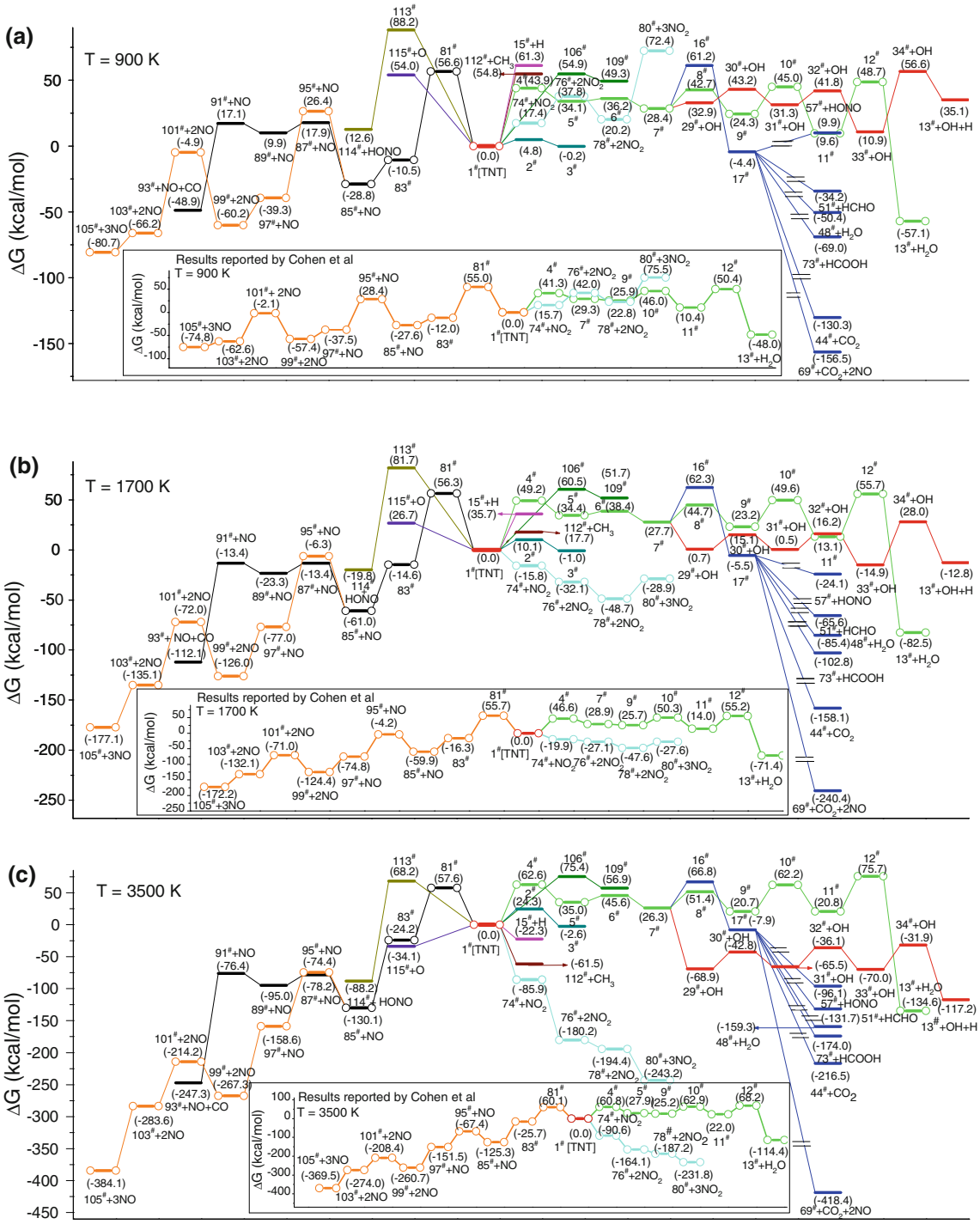

Fig. 8 Relative free energy (ΔG) diagram at higher temperatures (900, 1,700, and 3,500 K) for the decomposition and dissociation reactions of TNT, as calculated at uB3LYP/6-311++G(d,p). *Inset* illustrates the results reported by Cohen et al. at the uB3LYP/cc-PVDZ level. The *values in parenthesis* are the sum of electronic and thermal free energies (ΔG) at the specified temperature relative to TNT. *Each color line* represents one type of reaction route. The reaction routes are referred to Schemes 1, 2, and 3, but transition states and intermediates in the reactions of $17^{\#} \rightarrow 44^{\#} + CO_2$, $17^{\#} \rightarrow 48^{\#} + H_2O$, $17^{\#} \rightarrow 51^{\#} + HCHO$, $17^{\#} \rightarrow 57^{\#} + HONO$, $17^{\#} \rightarrow 69^{\#} + CO_2 + 2NO$, and $17^{\#} \rightarrow 73^{\#} + HCOOH$ are omitted for the sake of clarity, while their detailed information is provided in Fig. 9. The C–NO_2 homolysis and nitro-nitroso rearrangement of TNT in the *para* position, and two optional processes in the O elimination and nitro oxidizing adjacent backbone carbon atom pathways are omitted for the sake of clarity, and their detailed information are provided in supplementary material. *The lines with cycles* mean that the corresponding species were mentioned by Cohen et al.

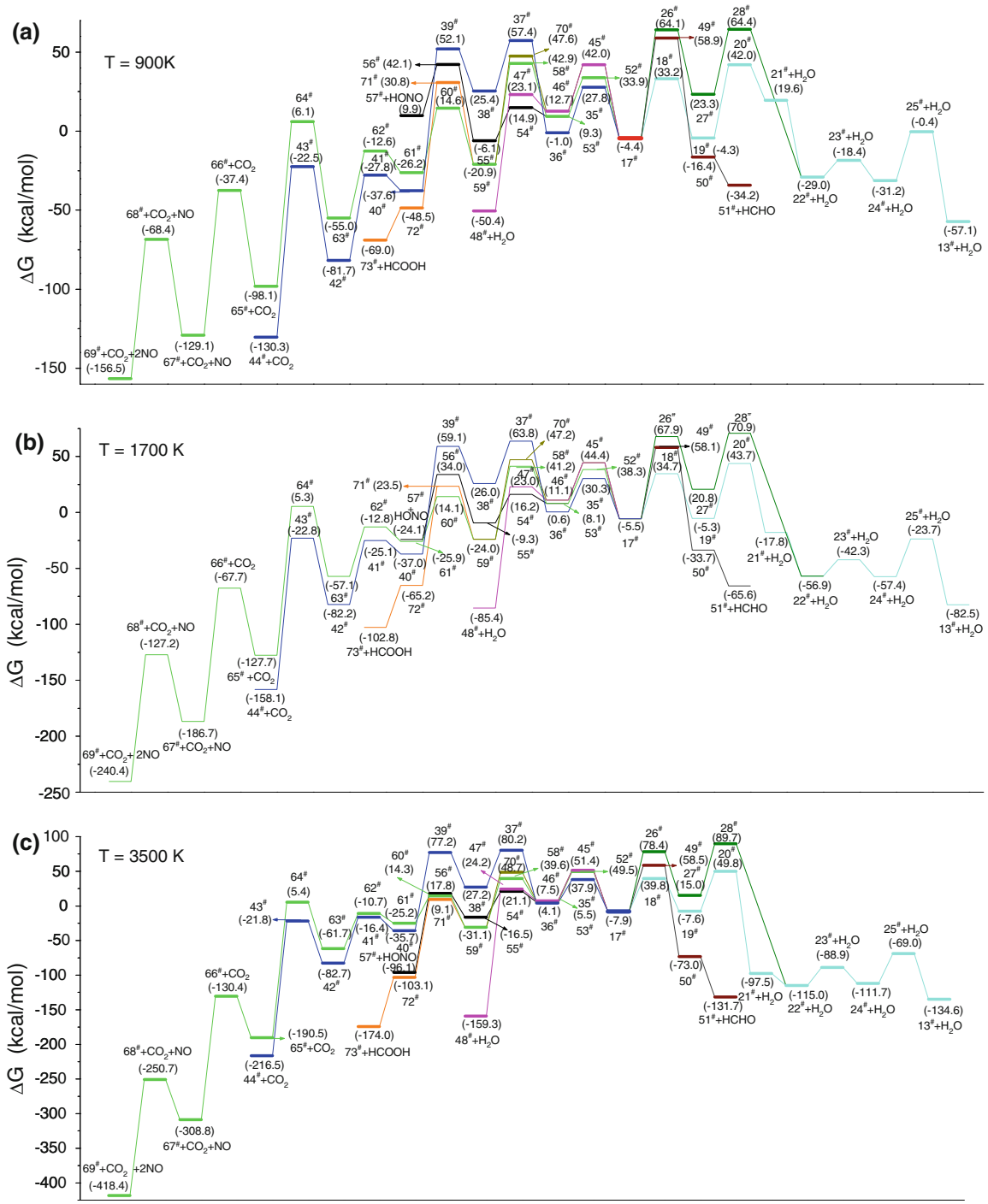

Fig. 9 Relative free energy (ΔG) diagram at higher temperatures (900, 1,700, and 3,500 K) for the degradation of the important intermediate 4,6-dinitro-2-nitroso-benzyl alcohol (*17*) during TNT decomposition, as calculated at uB3LYP/6-311++G(d,p). The *values in parenthesis* are the sum of electronic and thermal free energies (ΔG) at the specified temperature relative to TNT. The reaction routes are referred to Schemes 1 and 2

from the electron-donating effect of *ortho* methyl group. Therefore, Fig. 4 only provides the energy diagram for the dominant nitro-nitrite isomerization of TNT in the *ortho* position.

The subsequent nitro-nitrite isomerization–homolysis of the two remaining substituents in TNT will occur. As shown in Fig. 4, the rate-determining steps are TS_{42} (*95*) and TS_{44} (*101*) for the second and third nitro-nitrite

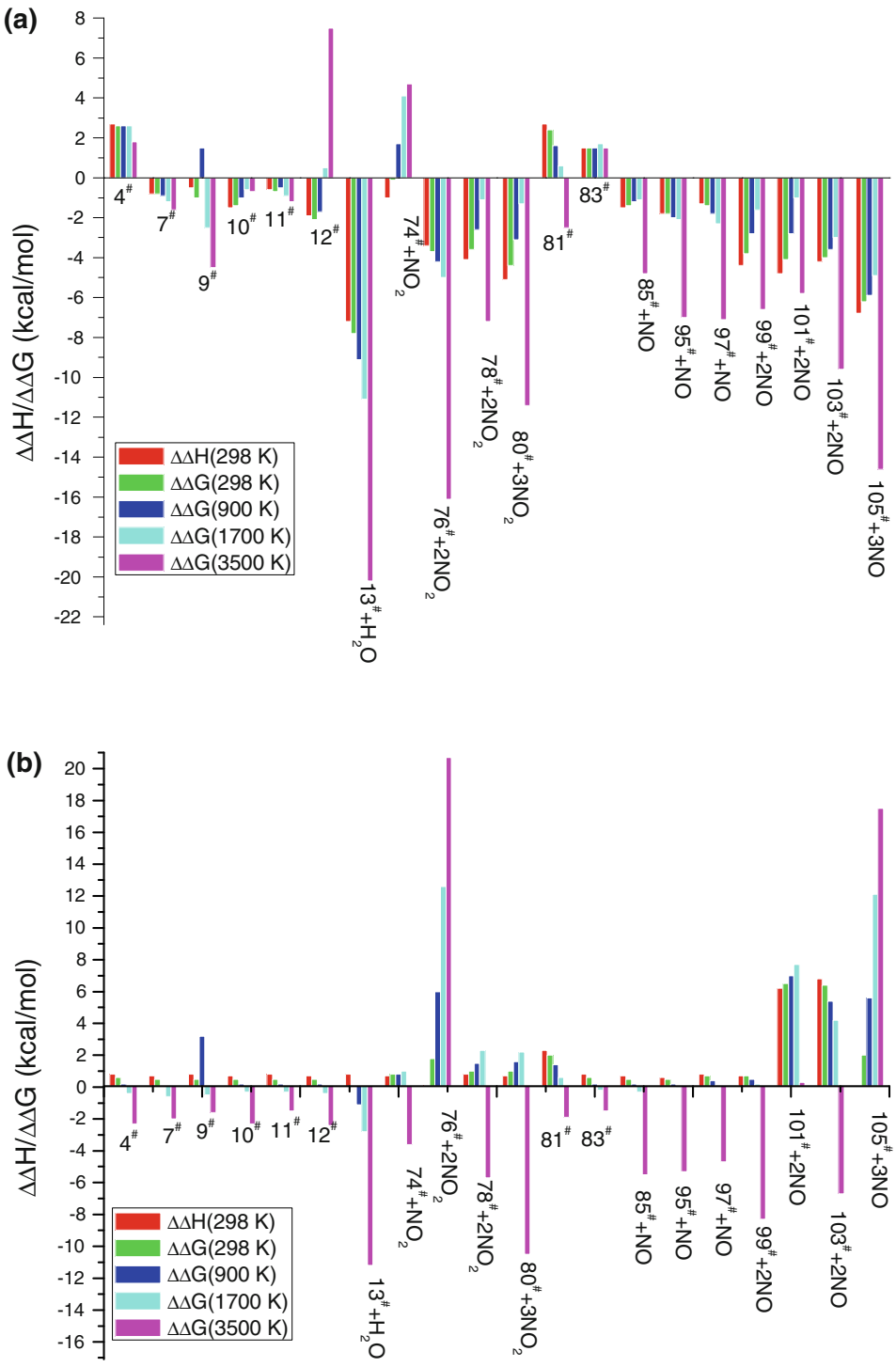

Fig. 10 The enthalpy/Gibbs free energy differences ($\Delta\Delta H(T)/\Delta\Delta G(T)$) at the specified temperature (T) between ours and Cohen et al.'s. All energies include thermal correlations. **a** At the different calculation level (ours: uB3LYP/6-311++G(d,p); Cohen et al.'s: uB3LYP/cc-PVDZ). **b** At the same calculation level (uB3LYP/cc-PVDZ)

isomerization–homolysis of TNT via the radical 3,5-dinitro-2-methyl phenoxy (*85*), with the enthalpies of 64.9 and 73.5 kcal/mol at 298 K relative to TNT. It is well known that phenoxy is likely to decompose into CO + cyclopentadienyl. The substituted phenoxy, 3,5-dinitro-2(or 4)-methyl phenoxy [*85* or (*86*)] will show some feature in common with phenoxy, as shown in Scheme 3. The rate-determining steps are TS_{38} (*87*) for the degradation of 3,5-dinitro-2-methyl phenoxy into CO + substituted-cyclopentadienyl (*93*), with the enthalpy barrier of 55.3 kcal/mol at 298 K relative to TNT.

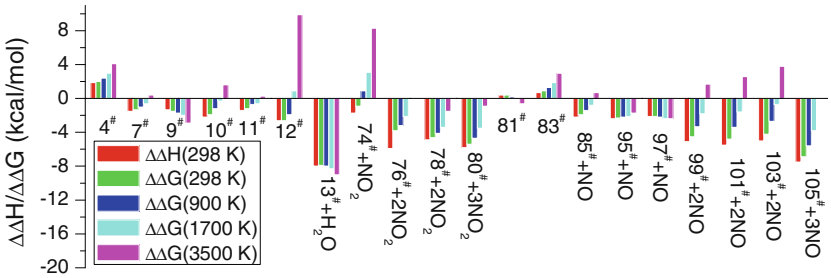

Fig. 11 The enthalpy/Gibbs free energy differences ($\Delta\Delta H(T)/\Delta\Delta G(T)$) at the specified temperature (T) calculated by us. All energies include thermal correlations. Noting that $\Delta\Delta H(T)/\Delta\Delta G(T)$ equals to the enthalpy/Gibbs free energy at the uB3LYP/6-311++G(d,p) level minus the enthalpy/Gibbs free energy at the uB3LYP/cc-PVD level at the specified temperature (T)

3.2.4 *Nitro group oxidizing adjacent backbone carbon*

The nitro group in TNT can oxidize adjacent benzene ring backbone carbons via ordered four-membered ring activation compounds (*106*, *107*, and *108*), shown in Fig. 3. The activated enthalpy barriers (ΔH) at 298 K are only 49.9, 50.6, and 59.2 kcal/mol, respectively. In addition, the products *109*, *110*, and *111* are above TNT in enthalpy (ΔH) at 298 K by 46.5, 45.9 and 55.1 kcal/mol, respectively.

3.2.5 *HONO elimination, methyl removal, H escape, and O elimination*

A medium-intense peak at *m*/*z* 180 in experiments [21, 22] is assumed to arise only from the loss of NO_2 and H in two steps. However, in spectrum of *o*-nitrotoluene, intensity at the parent mass unit is suggested to include contributions from two separate processes: one is that the elements of HNO_2 are lost as a unit or possibly as NO_2 and H; the other is that lost OH and NO occurs in two steps. Our results indicate that the elements of HNO_2 are possibly lost as a unit in the neutral molecule of TNT. As calculated, the *ortho* nitro group plus one of H atom in methyl group is separated from TNT via TS_{49} (*113*), with an enthalpy barrier (ΔH) at 298 K of 95.2 kcal/mol. The ion at *m*/*z* 180 may possibly be the product *114* losing one electron in so-called tropylium configuration. In addition, the Ph–CH_3, $PhCH_2$–H, and –CN(O)=O bonds are tight in TNT, and their bond dissociation enthalpies at 298 K are predicted to be 97.1, 87.1, and 84.2 kcal/mol in Fig. 4, respectively. Therefore, CH_3 removal, O elimination, and H escape is difficult to occur at room temperature.

3.3 Temperature dependence of relative importance of all possible pathways during TNT decomposition

The activation/reaction free energy is standard criteria to estimate roughly the relative importance of several paths of TNT decomposition. Figures 6 and 7 reveal that, at room temperature (298 K), TNT condensing to DNAt (*13*) by dehydration is kinetically the most favorable process with the lowest activation free energy (44.9 kcal/mol) in RDS and numerous net free energy releases (36.9 kcal/mol); parallel to DNAt in intra-H transfer path, species, *44*, *48*, *51*, *69*, and *73*, are all readily condensed from TNT, with net free energy releases (108.4, 23.5, 9.3, 89.8, and 42.4 kcal/mol, respectively), but they necessitate surmounting the higher activation free energy (60.6 kcal/mol) in RDS (*16*), therefore, species *44*, *48*, *51*, *69*, and *73*, are all the thermodynamic controlling products; nitro-nitrite rearrangement–homolysis leading to 3,5-dinitro-2-methyl phenoxy (*85*) gives the unique kinetic free energy (−3.9 kcal/mol), overcoming an higher activation free energy (57.3 kcal/mol), and it is the secondary pathway; TNT condensing to DNAt by losing OH and H, nitro group oxidizing adjacent backbone carbon, simple C–NO_2 homolysis, HONO elimination, methyl removal, O elimination, and H escape paths, will not occur, because all are endoergic processes (70.9, 47.4 (*ortho*), 43.7 (*ortho*), 38.3, 83.3, 74.5, and 79.5 kcal/mol, respectively), so will the extensive fragmentation of the substituted phenxyl.

However, Table 1 indicates, at room temperature, all exoergic paths mentioned above are with the activation entropy gains, except nitro group oxidizing adjacent backbone carbon path: the first, second, and third C–NO_2 homolysis in the *ortho*/*para* position, 44.6/43.6, 93.9/87.5, and 136.2/136.2 eu, respectively; loss of H, 27.2 eu; HONO elimination in the RDS (*113*), 7.4 eu; methyl removal, 46.3 eu; the second and third nitro-nitrite isomerization–homolysis in the RDS (*95*/*96* and *101*/*102*, respectively), 42.6/41.6 and 84.9/82.2 eu, respectively; loss of CO from 3,5-dinitro-2 (or 4)-methyl phenoxy in the RDS [*87* or (*88*), 41.9 (or 40.6] eu, respectively. In general, the enthalpy/entropy of a reaction varies slightly with temperature. It is easily proposed that the activation Gibbs free energies in those paths will become more and more negative with the temperature increasing, according to the expression of $\Delta G = \Delta H - T\Delta S$. In contrast, DNAt (*13*) condensed from TNT by dehydration possess the

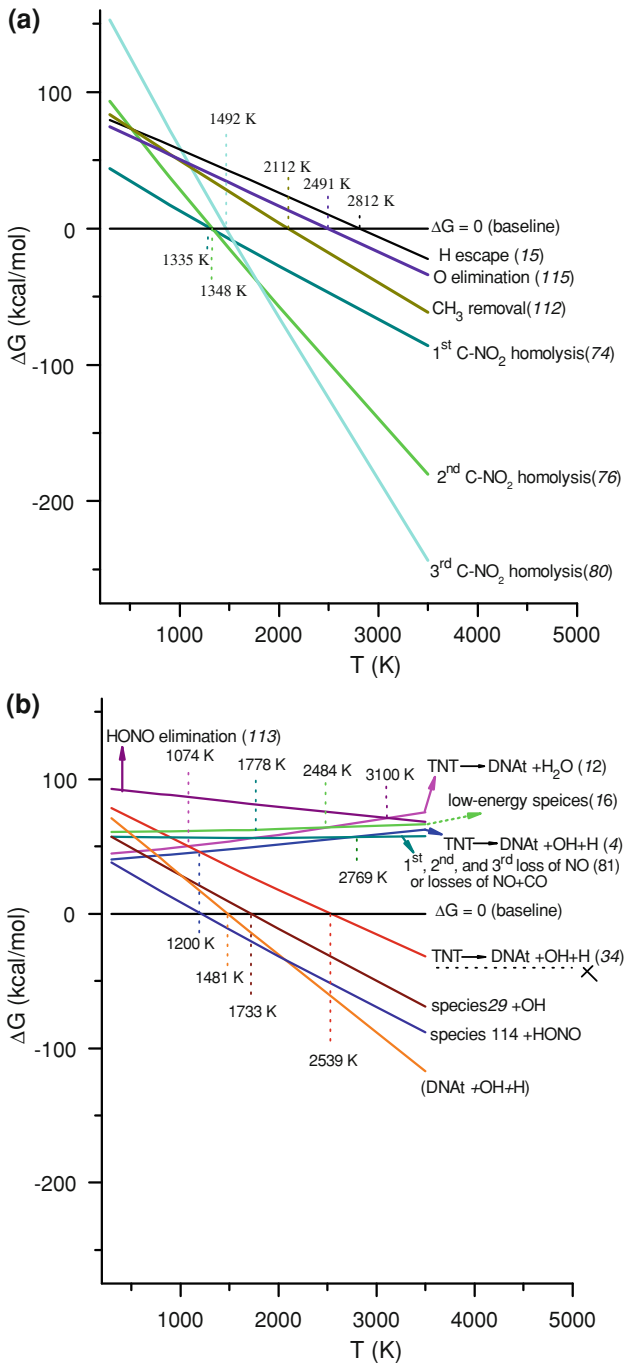

Fig. 12 The dependence between relative Gibbs free energy (ΔG) and temperature (T). The *values in parenthesis* designate the names of species in the rate-determining step (RDS). **a** For the dissociation reactions of TNT decomposition; **b** for DNAt production, nitro-nitrite rearrangement–homolysis, and HONO elimination paths

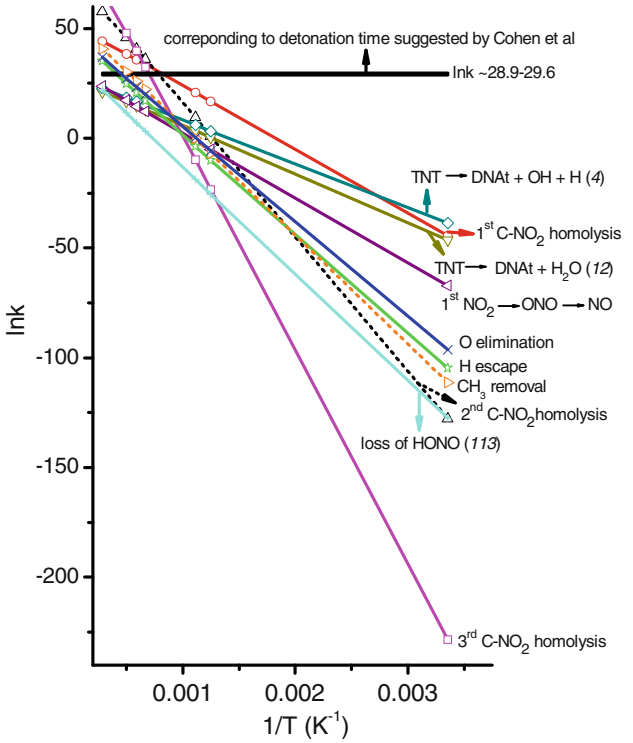

Fig. 13 Arrhenius plot (ln k vs. $1/T$) for TNT decomposition pathways. ln k values are calculated from the Eyring equation (Eq. 1) in which the ΔG for each pathway is assumed to be the RDS at the specified temperature

increasing activation free energy, due to the entropy loss (5.0 eu) in the RDS (*12*).

We obtained thermal corrections to the enthalpy, entropy and Gibbs free energy (based on the RRHO approximation) at different temperatures, using the *freqchk* utility of the *Gaussian 03* program [32]. Five higher temperatures (800, 900, 1,700, 2,000, and 3,500 K) are chosen for comparing with the available results reported by Cohen et al. [29].

The Gibbs free energy diagrams at three higher temperature (900, 1,700, and 3,500 K) in Figs. 8 and 9 indicate that (1) at 900 K, nitro group oxidizing adjacent backbone carbon, the first, second and third C–NO_2 homolysis, H escape, HONO elimination, and methyl removal paths are still endoergic processes; at 1,700 K, the C–NO_2 homolysis and HONO elimination paths already become exoergic processes; at 3,500 K, methyl removal, O elimination, and H escape paths also have negative Gibbs free energies of activation, (2) DNAt condensed from TNT is still both kinetically and thermodynamically dominated by dehydration at 900 K, but this situation changes, and the sequential losses of OH and H from TNT kinetically bears major responsibility for DNAt production at 1,700 K; (3) the intermediates, 3,5-dinitro-2-methyl phenoxy (*85*), is kinetically more favor to decompose into CO and 3,5-dinitro-2-methyl cyclopentadienyl (*93*) than to loss NO following nitro-nitrite rearrangement, even if at 3,500 K; (4) the species *16*, is still the RDS for the low-energy species *48*, *51*, *57*, *69*, and *73* even if the temperature reaches 3,500 K; but it switches to the species *37* for

Table 1 Relative entropies (ΔS) at 298 K for some important species during TNT decomposition, as calculated at the uB3LYP/6-311++G(d,p) level

Species[a,d]	ΔS	Species[b,d]	ΔS	Species[c,d]	ΔS
1	0.0	*1*	0.0	*1*	0.0
4	−5.7	*16*	−1.7	*15* + H	27.2
5	−1.7	*17*	0.7	*74/75* + NO_2	44.6/43.6
6	−2.0	*37*	−5.7	*76/77* + $2NO_2$	93.9/87.5
7	−0.7	*44* + CO_2	36.9	*80* + $3NO_2$	136.2
8	−2.7	*45*	−3.4	*81/82*	1.0/0.3
9	−0.3	*48* + H_2O	43.6	*83/84*	3.7/3.0
10	−5.0	*49*	1.3	*85/86* + NO	41.3/41.3
11	−4.7	*50*	19.1	*87/88* + NO	41.9/40.6
12	−5.0	*51* + HCHO	41.9	*91/92* + NO	40.6/41.9
13 + H_2O	33.9	*58*	0.0	*95/96* + NO	42.6/41.6
14	−2.3	*59*	1.7	*101/102* + 2NO	84.9/82.2
16	−1.7	*69* + CO_2 + 2NO	113.0	*106*	−5.0
17	0.7	*71*	8.0	*109*	−3.0
34 + OH	34.9	*72*	17.8	*112* + CH_3	46.3
13 + OH + H	57.4	*73* + HCOOH	44.9	*113*	7.4
				114 + HONO	42.9
				115 + O	32.5

Unit: eu

[a] The species correlate with TNT condensing to 4,6-dinitroanthranil (*13*)

[b] The species correlate with TNT degraded into some low-energy product systems through 4,6-dinitro-2-nitroso-benzyl alcohol (*17*)

[c] The species correlate with the loss of H, C–NO_2 homolysis, nitro-nitrite isomerization, nitro oxidizing adjacent backbone carbon atom, HONO elimination, methyl removal, and O elimination paths during TNT decomposition

[d] The reaction routes are referred to Schemes 1, 2 and 3

3,5-dinitroanline (*44*) production when the temperature is 1,700 or 3,500 K; nevertheless, those product systems (*44, 48*, *51*, *57*, *69*, and *73*) necessitate surmounting the higher activation free energy in RDS, although releasing numerous reaction free energies.

Insets in Figs. 4, 6, and 8 illustrate the previous theoretical results on the C–NO_2 homolysis, DNAt condensed from TNT by dehydration, and nitro-nitrite rearrangement–homolysis, as calculated at uB3LYP/cc-PVDZ level by Cohen et al. [29]. Those are only the subset of all possible pathways of TNT decomposition. Cohen et al. proposed that the reaction route for TNT condensing to DNAt is TNT (*1*) → *7* → *9* → *10* → *11* → *12* → *13* (DNAt) + H_2O. This route is similar to our suggested one with the lowest Gibbs free energy at room temperature, i.e., TNT (*1*) → *4* → *5* → *6* → *7* → *8* → *9* → *10* → *11* → *12* → *13* (DNAt) + H_2O. However, species, *5*, *6*, and *8*, were obtained by performing the necessary intrinsic reaction coordinates calculations. In addition, one more favorable degradation of the intermediates, 3,5-dinitro-2-methyl (*85*) phenoxy into CO and substituted cyclopentadienyl was not explored by Cohen et al. [29]. For the common species, their enthalpies and Gibbs free energies in Figs. 4, 6, and 8 are slightly different between Cohen et al. and ours, which are generally within 1–4 kcal/mol as shown in Fig. 10a. However, we did not understand the larger discrepancies in Gibbs free energies at 3,500 K and in products systems involving species *13*, *76*, *101*, *103*, and *105*. To interpret this abnormality, we also calculated these species at the uB3LYP/cc-PVDZ level, using atom coordinates provided by Cohen et al. as the initial guess. Even at the same level, the abnormality does not disappear, as shown in Fig. 10b. However, Fig. 11 indicates that our calculated enthalpies/Gibbs free energies at the two different levels agree highly with each other at all temperatures.

To determine threshold temperatures, the dependence between the activation/reaction Gibbs free energy (ΔG) versus temperature (T) is provided in Fig. 12. Some threshold temperatures at which the activation Gibbs free energy in the RDS become zero in Fig. 12a are: first C–NO_2, ~1,335 K, second C–NO_2, ~1,348 K, third C–NO_2, ~1,492 K (only considering the C–NO_2 homolysis of TNT in the *ortho* position); CH_3 removal, ~2,112 K; O elimination, ~2,491 K; H escape, ~2,812 K. Figure 12b indicates that RDS of TNT → DNAt + OH + H changes from the species *34* to *4* when the temperature is above

~1,200 K, and then it is species *4* when this reaction becomes exoergic above ~1,481 K, therefore, DNAt production by sequential losses of OH and H kinetically favors over by dehydration above ~1,481 K; the nitro-nitrite rearrangement–homolysis kinetically becomes more favorable to DNAt production above ~1,778 K by dehydration and above ~2,769 K by sequential losses of OH and H; HONO eliminating directly from TNT becomes exoergic above ~1,200 K, this process is always with the highest activation Gibbs free energy when the temperature ranges from 298 to 3,100 K.

Cohen et al. have estimated detonation time scale of ~100–200 fs, which derived from the detonation rate of TNT (~6,900 m/s) and the size of the TNT unit cell in the bulk (10–20 Å) [24, 29–31]. They inferred that the ln k values for detonation with the half-life time ($t_{1/2}$) in the range of 100–200 fs are 29.6–28.9, and further determined that only the C–NO_2 homolysis takes place at the detonation time, based on Eqs. 1 and 2.

$$k = \frac{k_B T}{h} e^{-\Delta G^{\neq}/RT} \quad (1)$$

$$t_{1/2} = \frac{\ln 2}{k} \quad (2)$$

where k is the rate, k_B is Boltzmann's constant, h is Planck's constant, $\Delta G^{\neq}$ is the activation Gibbs free energy barrier in the RDS, R is the gas constant, T is the temperature in Kelvin, and $t_{1/2}$ is the half-life time (s).

The C–NO_2 homolysis, DNAt condensed from TNT by dehydration, and nitro-nitrite rearrangement–homolysis were only considered by Cohen et al. [29]. Below will examine all possible pathways of TNT decomposition we suggested, according to their employed kinetic analysis. In Arrhenius plot (ln k vs. $1/T$) for TNT decomposition, the pathways cross the window of the ln k values (29.6–28.9) represent they are kinetically accessible during TNT detonation specific temperatures. Obviously, another three pathways, CH_3 removal, O elimination, and H escape, cross the window of these ln k values (29.6–28.9) in Fig. 13, besides the first, second, and third C–NO_2 homolysis.

Hereto, 20 main unimolecular decomposition and dissociation reactions of TNT have been emphasized in this study, which derived from seven possible pathways, as shown in Table 2. Their relative importance at each temperature is concluded in Table 3. (1) Below ~1,335 K, DNAt condensed from TNT by dehydration is kinetically the most favor process, and loss(es) of NO or NO + CO stemmed from nitro-nitrite rearrangement includes the minor contribution to TNT decomposition, and the thermodynamically controlling products (*44, 48, 51, 57, 69,* and *73)* formation kinetically plays the least role in TNT

Table 2 Most important unimolecular decomposition and dissociation reactions of TNT

Pathway	Reaction	
Intra-H transfer	TNT → 4,6-dinitroanthranil (DNAt) + H_2O	Eq. 1
	TNT → DNAt + OH + H	Eq. 2
	TNT → 4,6-dinitro-2-nitroso-benzyl alcohol (*17*)	Eq. 3
	TNT → 3,5-dinitroaniline (*44*) + CO_2	Eq. 4
	TNT → 2,6-dinitroso-4-nitro-phenyl aldehyde (*48*) + H_2O	Eq. 5
	TNT → 3,5-dinitro-1-nitrosobenzene (*51*) + HCHO	Eq. 6
	TNT → 2-formyl-3-nitrosimino-5-nitro-phenyl (*57*) + HONO	Eq. 7
	TNT → nitrobenzene (*69*) + CO_2 + 2NO	Eq. 8
	TNT → 3,5-dinitroso-1-nitrobenzene (*73*) + HCOOH	Eq. 9
First C–NO_2 homolysis	TNT → 3,5-dinitro-2-methyl phenyl (*74*) + NO_2	Eq. 10
Second C–NO_2 homolysis	TNT → di-radical $CH_3C_6H_2NO_2$ (*76*) + $2NO_2$	Eq. 11
Third C–NO_2 homolysis	TNT → tri-radical $CH_3C_6H_2$ (*80*) + $3NO_2$	Eq. 12
Nitro-nitrite rearrangement–fragmentation	TNT → 3,5-dinitro-2-methyl phenoxy (*85*) + NO	Eq. 13
	TNT → 3,5-dinitro-2-methyl-cyclopentadienyl + NO + CO	Eq. 14
	TNT → di-radical $CH_3(NO_2)(O)C_6H_2O$ (*99*) + 2NO	Eq. 15
	TNT → tri-radical $CH_3(O)C_6H_2O(O)$ (*105*) + 3NO	Eq. 16
H escape	TNT → 2,4,6-trinitro-benzyl (*15*) + H	Eq. 17
CH_3 removal	TNT → 2,4,6-trinitro-phenyl (*115*) + CH_3	Eq. 18
HONO elimination	TNT → $(O_2N)_3CH_3C_6H_2(CH_2)$ (*114*) + HONO	Eq. 19
O elimination	TNT → 2,4-dinitro-6-(*cis*)-nitroso-toluene (*115*) + O	Eq. 20

Note that the italic values in parenthesis represent the names of species in Fig. 3

Table 3 Relative importance of all possible pathways of TNT decomposition at each temperature (298–3,500 K) in kinetic opinion

Temperature (T)	Relative importance
$T <$ ~1,200 K	Eq. 1 $\gg$ Eqs. 13–16 > Eqs. 3–9
~1,200 K $< T <$ ~ 1,335 K	Eq. 1 $\gg$ Eqs. 13–16 > Eqs. 3–9 > Eq. 19
~1,335 K $< T <$ ~ 1,481 K	Eqs. 10, 11 $\gg$ Eq. 1 > Eqs. 13–16 > Eqs. 3–9
~1,481 K $< T <$ ~ 1,778 K	Eqs. 10–12 $\gg$ Eq. 2 > Eq. 1 > Eqs. 13–16 > Eqs. 3–9
~1,778 K $< T <$ ~ 2,112 K	Eqs. 10–12 $\gg$ Eq. 2 > Eqs. 13–16 > Eq. 1 > Eqs. 3–9
~2,112 K $< T <$ ~ 2,484 K	Eqs. 10–12 > Eq. 18 $\gg$ Eq. 2 > Eqs. 13–16 > Eq. 1 > Eqs. 3–9
~2,484 K $< T <$ ~ 2,491 K	Eqs. 10–12 > Eq. 18 $\gg$ Eq. 2 > Eqs. 13–16 > Eqs. 3–9 > Eq. 1
~2,491 K $< T <$ ~ 2,769 K	Eqs. 10–12 > Eq. 18 > Eq. 20 $\gg$ Eq. 2 > Eqs. 13–16 > Eqs. 3–9 > Eq. 1
~2,769 K $< T <$ ~ 2,812 K	Eqs. 10–12 > Eq. 18 > Eq. 20 $\gg$ Eq. 2 > Eqs. 13–16 > Eqs. 3–9 > Eq. 1
$T >$ ~2,812 K	Eqs. 10–12 > Eq. 18 > Eq. 20 > Eq. 17 $\gg$ Eq. 2 > Eqs. 13–16 > Eq. 1 > Eqs. 3–9

The reaction equations (Eq. x) are shown in Table 2

decomposition until HONO elimination becomes exoergic above ~1,200 K, but the other paths with the endothermicity do not occur. (2) Above ~1,335 K, simple C–NO_2 homolysis kinetically dominates TNT decomposition. When the temperature ranges from ~1,335 to 2,112 K, the secondary and minor contributions are attributed to DNAt production and 3,5-dinitro-2-methyl phenoxy productions following degeneration, respectively. DNAt condensed from TNT by dehydration yields to that by sequential losses of OH and H above ~1,481 K and to nitro-nitrite rearrangement–homolysis above ~1,778 K. Above ~2,112 K, CH_3 removal becomes kinetically the secondary process. O atom elimination includes tertiary contribution to TNT decomposition above ~2,491 K. H escaping directly from TNT starts to play the fourth role in TNT decomposition above ~2,812 K. (3) Species, *44, 48, 51, 57, 69,* and *73*, are thermodynamically controlling at all temperatures. (4) At the estimated detonation times (100–200 fs), four pathways contribute to the detonation of TNT, which are the C–NO_2 homolysis; CH_3 removal, O elimination, and H escape in order of the decreasing importance. (5) Nitro group oxidizing adjacent backbone carbon path with endothermicity could not occur at all temperatures.

4 Conclusions

Thermal reactions of TNT have been explained in terms of its initial decomposition. In addition, initial detonation stage of TNT is evidently involved in eight major types of mechanisms. The relative importance of several initiation processes was estimated roughly. To clarify the origins of some identified products in experiments, some processes characterizing those sequential decompositions of TNT have been further investigated in considerable detail and such mechanistic details as well as competing processes have also been the central subject in this article.

Acknowledgments We thank the supercomputer center of Virtual Laboratory of Computational Chemistry, Computer Network Information Center, Chinese Academy of Sciences for the computational resources. This research was supported by the National Key Basic Research Special Foundation (NKBRSF 2007CB815202).

References

1. Urbanski T (1984) Chemistry and technology of explosives. Pergamon Press, New York
2. Brill TB, James KJ (1993) Chem Rev 93:2667
3. Ledingham KWD, Kilic HS, Kosmidis C, Deas RM, Marshall A, McCanny T, Singhal RP, Langley AJ, Shaikh W (1995) Rapid Commun Mass Spectrom 9:1522
4. Rogers RN (1967) Anal Chem 39:730
5. Miles MH, Gustaveson D, Devries KL (1983) J Mater Sci 18:3243
6. Menapace JA, Marlin JE (1990) J Phys Chem 94:1906
7. Patterson JM, Shiue C-Y, Smith WT Jr (1973) J Org Chem 38:2447
8. Feinstein A, Fields EK (1971) J Org Chem 36:3878
9. Morrison H, Migdalof BH (1965) J Org Chem 30:3996
10. Brill TB, James KJ (1993) J Phys Chem 97:8759
11. Dacons JC, Adolph HG, Kamlet MJ (1970) J Phys Chem 74:3035
12. Shackelford SA, Beckmann JW, Wilkes JS (1977) J Org Chem 42:4201
13. Janzen EG (1965) J Am Chem Soc 87:3531
14. Guidry RM, Davis LP (1979) Thermochim Acta 32:1
15. Davis LP, Wilkes JS, Pugh HL, Dorey RC (1981) J Phys Chem 85:3505
16. McKinney TM, Warren LF, Goldberg IB, Swanson JT (1986) J Phys Chem 90:1008
17. Burlinson NE, Sitzman ME, Kaplan LA, Kayser E (1979) J Org Chem 44:3695
18. Zitrin S, Yinon J (1976) Org Mass Spectrom 11:388
19. Carper WR, Dorey RC, Tomer KB, Crow FW (1984) Org Mass Spectrom 19:623
20. Yinon J (1987) Org Mass Spectrom 22:501
21. Yinon J, McClellan JE, Yost RA (1997) Rapid Commun Mass Spectrom 11:1961
22. Hankin SM, Tasker AD, Robson L, Ledingham KWD, Fang X, McKenna P, McCanny T, Singhal RP, Kosmidis C, Tzallas P,

Jaroszynski DA, Jones DR, Issac RC, Jamison S (2002) Rapid Commun Mass Spectrom 16:111
23. Martin AN, Farquar GR, Gard EE, Frank M, Fergenson DP (2007) Anal Chem 79:1918
24. Carper WR, Davis LP, Extine MW (1982) J Phys Chem 86:459
25. Clarkson J, Smith WE, Batchelder DN, Smith DA, Coats AM (2003) J Mol Struct 648:203
26. Turner AG, Davis LP (1984) J Am Chem Soc 106:5447
27. Turner AG (1986) J Phys Chem 90:6000
28. Cox JR, Hillier IH (1988) Chem Phys 124:39
29. Cohen R, Zeiri Y, Wurzberg E, Kosloff R (2007) J Phys Chem A 111:11074
30. Golovina NI, Titkov AN, Raevskii AV, Atovmyan LO (1994) J Solid State Chem 113:229
31. Vrcelj RM, Sherwood JN, Kennedy AR, Gallagher HG, Gelbrich T (2003) Cryst Growth Des 3:1027
32. Frisch MJ, Trucks GW, Schlegel HB, Scuseria GE, Robb MA, Cheeseman JR, Montgomery JA Jr, Vreven T, Kudin KN, Burant JC, Millam JM, Iyengar SS, Tomasi J, Barone V, Mennucci B, Cossi M, Scalmani G, Rega N, Petersson GA, Nakatsuji H, Hada M, Ehara M, Toyota K, Fukuda R, Hasegawa J, Ishida M, Nakajima T, Honda Y, Kitao O, Nakai H, Klene M, Li X, Knox JE, Hratchian HP, Cross JB, Adamo C, Jaramillo J, Gomperts R, Stratmann RE, Yazyev O, Austin AJ, Cammi R, Pomelli C, Ochterski JW, Ayala PY, Morokuma K, Voth GA, Salvador P, Dannenberg JJ, Zakrzewski VG, Dapprich S, Daniels AD, Strain MC, Farkas O, Malick DK, Rabuck AD, Raghavachari K, Foresman JB, Ortiz JV, Cui Q, Baboul AG, Clifford S, Cioslowski J, Stefanov BB, Liu G, Liashenko A, Piskorz P, Komaromi I, Martin RL, Fox DJ, Keith T, Al-Laham MA, Peng CY, Nanayakkara A, Challacombe M, Gill PMW, Johnson B, Chen W, Wong MW, Gonzalez C, Pople JA (2004) Gaussian 03, revision C02. Gaussian, Inc, Wallingford
33. Lee C, Yang W, Parr RG (1988) Phys Rev B 37:785
34. Becke AD (1992) J Chem Phys 96:2155
35. Becke AD (1992) J Chem Phys 97:9173
36. Becke AD (1993) J Chem Phys 98:5648
37. McLean AD, Chandler GS (1980) J Chem Phys 72:5639
38. Krishnan R, Binkley JS, Seeger R, Pople JA (1980) J Chem Phys 72:650
39. Clark T, Chandrasekhar J, Spitznagel GW, Schleyer PvR (1983) J Comput Chem 4:294
40. Wu CJ, Fried LE (1997) J Phys Chem A 101:8675
41. Chakraborty D, Muller RP, Dasgupta S, Goddard WA (2000) J Phys Chem A 104:2261
42. Chakraborty D, Muller RP, Dasgupta S, Goddard WA (2001) J Phys Chem A 105:1302
43. Alavi S, Reilly LM, Thompson DL (2003) J Chem Phys 119:8297
44. Lynch BJ, Truhlar DG (2001) J Phys Chem A 105:2936
45. Merrick JP, Moran D, Radom L (2007) J Phys Chem A 111:11683
46. Andersson MP, Uvdal P (2005) J Phys Chem A 109:2937
47. Frisch MJ, Pople JA, Binkley JS (1984) J Chem Phys 80:3265
48. Gonzalez C, Schlegel HB (1989) J Chem Phys 90:2154
49. Gonzalez C, Schlegel HB (1990) J Phys Chem 94:5523
50. Eckert F, Rauhut G (1998) J Am Chem Soc 120:13478
51. Lifshitz A, Tamburu C, Suslensky A, Dubnikova F (2006) J Phys Chem A 110:8248
52. Gonzalez AC, Larson CW, McMillen DF, Golden DM (1985) J Phys Chem 89:4809
53. Fields EK, Meyerson S (1968) J Org Chem 33:4487
54. Fields EK, Meyerson S (1968) Tetrahedron Lett 10:1201
55. Fields EK, Meyerson S (1965) Adv Free Radic Chem 5:101
56. Schmidt A-C, Herzschuh R, Matysik F-M, Engewald W (2006) Rapid Commun Mass Spectrom 20:2293
57. Tomer KB, Gebreyesus T, Djerassi C (1973) Org Mass Spectrom 7:383
58. Tsang W, Robaugh D, Mallard WG (1986) J Phys Chem 90:5968
59. He YZ, Cui JP, Mallard WG, Tsang W (1988) J Am Chem Soc 110:3754
60. Fayet G, Joubert L, Rotureau P, Adamo C (2008) J Phys Chem A 112:4054
61. Tanaka G, Weatherford C (2008) Int J Quantum Chem 108:2924
62. Brill TB, James KJ, Chawla R, Nicol G, Shukla A, Futrell JH (1999) J Phys Org Chem 12:819
63. Beynon JH, Bertrand M, Cooks RG (1973) J Am Chem Soc 95:1739
64. Xu S, Lin MC (2005) J Phys Chem B 109:8367